REPORT DOCUMENTATION PAGE

Form Approved OMB NO. 0704-0188

1. REPORT DATE (DD-MM-YYYY)	2. REPORT TYPE	3. DATES COVERED (From - To)
21-06-2009	Final Report	1-Jul-2006 - 30-Jun-2009

4. TITLE AND SUBTITLE

Shape Optimization of Plates to Mitigate the Effects of Air Blast Loading

5a. CONTRACT NUMBER

W911NF-06-1-0265

5b. GRANT NUMBER

5c. PROGRAM ELEMENT NUMBER

611102

6. AUTHORS

Ashok D. Belegundu

5d. PROJECT NUMBER

5e. TASK NUMBER

5f. WORK UNIT NUMBER

7. PERFORMING ORGANIZATION NAMES AND ADDRESSES

Pennsylvania State University
Office of Sponsored Programs
The Pennsylvania State University
University Park, PA   16802   -

8. PERFORMING ORGANIZATION REPORT NUMBER

9. SPONSORING/MONITORING AGENCY NAME(S) AND ADDRESS(ES)

U.S. Army Research Office
P.O. Box 12211
Research Triangle Park, NC 27709-2211

10. SPONSOR/MONITOR'S ACRONYM(S)

ARO

11. SPONSOR/MONITOR'S REPORT NUMBER(S)

50490-EG.1

12. DISTRIBUTION AVAILIBILITY STATEMENT

Approved for public release; Distribution Unlimited

13. SUPPLEMENTARY NOTES

The views, opinions and/or findings contained in this report are those of the author(s) and should not contrued as an official Department of the Army position, policy or decision, unless so designated by other documentation.

14. ABSTRACT

This report presents a formal approach for optimizing the shape of freely supported isotropic plates to withstand air blast loading. Unique difficulties are presented by the nature of short-duration dynamic loading, viz. transient dynamic response, monitoring of maximum plastic strain failure at every point in the panel over time, optimizers that can handle non-differentiable, nonconvex and computationally expensive functions, and mesh distortion. LS-DYNA is used as the finite element software. The finite element model has been developed to reflect

15. SUBJECT TERMS

optimization, shape, blast, plate, design, honeycomb

16. SECURITY CLASSIFICATION OF:			17. LIMITATION OF ABSTRACT	15. NUMBER OF PAGES	19a. NAME OF RESPONSIBLE PERSON
a. REPORT	b. ABSTRACT	c. THIS PAGE	SAR		Ashok Belegundu
U	U	U			19b. TELEPHONE NUMBER
					814-863-2115

Shape Optimization of Plates to Mitigate the Effects of Air Blast Loading

Author / Principal Investigator

Dr. Ashok D. Belegundu
Professor of Mechanical Engineering
Dept. of Mechanical & Nuclear Engineering
The Pennsylvania State University, University Park, PA 16802
330 Leonhard Bldg., University Park, PA 16802
adb3@psu.edu , phone: 814-863-2115

Program Monitor

Dr. Bruce LaMattina, bruce.lamattina@us.army.mil
Mechanical Sciences Division, Army Research Office

Project Title:
A Methodology to Design Multiphase, Graded Composites to Safeguard Against Erosion

Abstract

This report presents a formal approach for optimizing the shape of freely supported isotropic plates to withstand air blast loading. Unique difficulties are presented by the nature of short-duration dynamic loading, viz. transient dynamic response, monitoring of maximum plastic strain failure at every point in the panel over time, optimizers that can handle non-differentiable, nonconvex and computationally expensive functions, and mesh distortion. LS-DYNA is used as the finite element software. The finite element model has been developed to reflect experimental test conditions and observed structural response. The goal has been to minimize dynamic displacement relative to the fixture, while monitoring plastic strain values, mass, and envelope constraints. A Fortran code has been developed to implement the methodology. Sinusoidal basis shapes are used to obtain an optimized double-bulge shape. Importantly, the flat plate is associated with a concentration of plastic strain at its center while for the optimized bulge shape, the plastic strain is smeared around the support showing greater utilization of material. Results show that much superior structural systems can be designed compared to ad-hoc techniques that sometimes fail to improve even the baseline design of a flat plate. Change in optimized shape with increasing offset in charge location is studied. A methodology for optimizing honeycomb sandwich structures is presented, utilizing a novel technique for linking honeycomb core geometry with its stress-strain curve.

Keywords: optimization, shape, blast, plate, design

Table of Contents

Nomenclature

$\mathbf{x}$ = design variables vector
$\mathbf{x}^{\mathbf{L}}$ = lower limit on design variables
$\mathbf{x}^{\mathbf{U}}$ = upper limit on design variables
$\mathbf{G}$ = vector of x-, y-, z- coordinates of nodes in FE model
$\mathbf{q}^{i}$ = i th velocity field or trial shape change vector
w = z- or normal displacement
$\varepsilon_{\max}$ = maximum plastic strain at failure for the material
ε = equivalent plastic strain vector
M = total mass of the structure
$M_{\max}$ = upper limit for the mass of the structure
t = thickness of the structure (plate) at any (x, y) location in the plate
$t_{\min}$ = Minimum thickness allowed
$\mathbf{z}$ = vector of z-coordinate of the nodes
$\mathbf{z}^{\mathbf{U}}$ = upper limit on z-coordinate
$\mathbf{z}^{\mathbf{L}}$ = lower limit on z-coordinate
$(\det J_j)$ = Jacobian of j th hexahedral element at all the eight nodes

1. Introduction

This report presents an approach and methodology to optimize the shape of panels to mitigate the effect of air blast loading, which comprises of a short duration pressure pulse. Unique difficulties are presented by the nature of the blast loading, viz. transient dynamic response, modeling the experimental setup with appropriate boundary conditions, monitoring of maximum plastic strain failure at every point in the panel over time, and optimizers that can handle non-differentiable, nonconvex, and computationally expensive functions. Much superior structural shapes can be designed using a formal optimization methodology compared to using ad-hoc techniques.

Considerable attention in journals and conferences worldwide has been given to *analysis* of metallic and composite panels, subject to both blast and ballistic loads. Regarding designing for impact mitigation, much greater focus has been placed on ballistic impact rather than on blast. Very few papers use formal optimization techniques. Publications relating to blast damage mitigation are given below.

This report focuses on shape of isotropic metal plates. Dharaneepathy and Sudhesh [1] investigate stiffener patterns on a square plate subject to blast loads modeled using Friedlander's exponential function. While formal optimization was not used to optimize the stiffener patterns, they demonstrated that stiffeners do provide significant advantage compared to an unstiffened panel of same weight, and that a waffle pattern is not as good as a novel pattern that they proposed. Failure was not considered in their study – that is, only deflection was considered. Hou et al [2] also consider the effect of stiffener size on blast response. Xue and Hutchinson [3] and Fleck and Deshpande [4] compare blast resistance of solid versus sandwich panels (such as pyramidal truss core, square honeycomb and folded plate). The plates were considered to be infinitely long in one direction and fixed at the ends of the short direction. ABAQUS/Explicit was used to model the blast load in Ref. [3] while an approximate analytical approach was used in Ref. [4]. Blast in both air and water were included in the comparative study. From certain normalized displacement versus impulse graphs, it was concluded that some of the sandwich topologies outperformed solid panels of same mass, especially in water. Yen, Skaags and Cheeseman [5] present an experimentally validated dynamic analysis procedure utilizing Ls-Dyna and the ConWep air blast function with shock mitigation materials such as honeycomb or foam. The numerical results indicate that significant reduction in the maximum stress amplitude propagating within the protected components can be achieved by suitable selection of honeycomb material with proper crush strength. Liang, Yang and Wu [6] focused on static loading and hence not very relevant in the present context of blast effects where inertia effects play a role. Further, their paper ignores material nonlinearity. Main and Gazonas [7] study the effect of an air blast on uniaxial crushing of a cellular sandwich plates. They investigated the physics of shock mitigation for different geometries of the cellular core. Icardi and Ferrero [8] study optimum fiber orientations in a laminated composite to absorb energy while maintaining stiffness. Further details on effectiveness of blast mitigation solutions in a laboratory using the Pendulum Test are given in [5, 9, 10].

There are instances in the public domain that show the mitigating effects of the shape of the plate. For example, United States Patent 7357062 (http://www.freepatentsonline.com/7357062.html) shows that V-shape deflects blast waves away. We view the V-shape as a bulge towards the charge and belonging to the family of single- and double- bulges obtained in this formal optimization study. Our focus is on the development

of a methodology that can be applied to the design of any plate, i.e. not just aluminum plates, and design for any given amount of blast charge, location and any boundary conditions.

In contrast with the papers cited above, this report uses formal optimization techniques, focuses on solid metal plates, uses Ls-Dyna for simulation and considers plastic strain to failure in the metal. The methodology involves integrating an optimizer with the Ls-Dyna simulation code. In Section 2, we formulate the optimization problem. Ls-Dyna finite element modeling of blast loading is discussed in Section 3. Material properties are also given in Section 3. Sections 4-5 contain the shape optimization approach. Computer code development is discussed in Section 6, results in Section 7 and conclusions in Section 8. Clear improvement over a flat plate is demonstrated.

2. Problem Definition

The schematic diagram of the plate used for shape optimization is shown in Fig. 1. The standoff distance of the charge is taken to be 0.4064 m. It should be noted that plate is just a part of a freely supported 'grip' assembly used to model the experimental condition as explained in the next Section. With reference to Fig. 1, the basic problem addressed in this work can be stated as follows:

Given a set of basis shapes which controls the shape and thickness of the plate, a mass limit for the structure, plastic strain limits representing fracture strength, a minimum thickness for the panel, and a geometric envelope within which the structure must lie , determine the best possible combination of these basis shapes that minimizes the deflection (at the first peak in time).
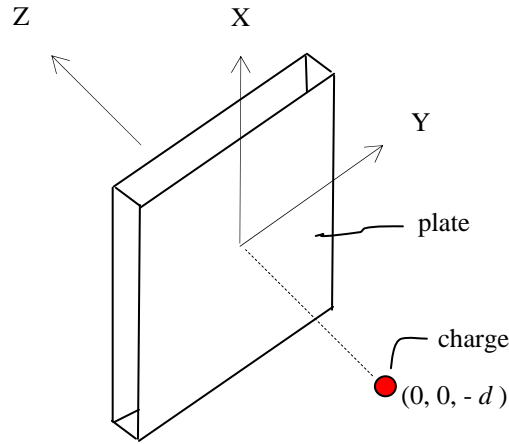

**Figure 1.   Baseline Structural Model: Plate dimensions are
(1.2192 m x 1.2192 m x 0.024 m), Standoff distance *d* = 0.4064 m**

Utilizing the already described notation, the problem can be formulated as follows.

$$\text{minimize} \quad \left\| w\left(\mathbf{x} \right) \right\|_r \tag{1}$$

subject to

$$\varepsilon_j \leq \varepsilon_{\max} \qquad \text{for each element } j$$
$$M \leq M_{\max}$$
$$t \geq t_{\min}$$
$$\mathbf{x}^{\text{L}} \leq \mathbf{x} \leq \mathbf{x}^{\text{U}}$$
$$det\ J_j\left(\mathbf{x} \right) \geq 0 \qquad \text{for each element } j$$
$$\mathbf{z}^{\text{L}} \leq \mathbf{z} \leq \mathbf{z}^{\text{U}} \qquad \text{(envelope)}$$

Important notes regarding the above problem are as follows.

(i)   Euclidean norm of the *relative* z-displacement of nodes in the plate is taken as the objective function (i.e. $r = 2$ in the objective function definition above). *x*- and *y*-displacements are not significant and are not considered. The term 'relative' is explained subsequently. The displacement is a function of time, and value at first peak is monitored.

(ii)   Plastic strain, also a function of time, stabilizes after a certain simulation time duration. This stabilized value is used in the constraint.

(iii)   *M* above refers to the combined mass of the assembly (Fig. 2).

(iv)   Thickness is computed from nodal coordinates of the <u>hexahedral elements</u> used in the FE model. Element distortion is prevented by computing determinant of Jacobian in every element and is forced to stay positive during optimization. The Jacobian for each element is computed from element nodal coordinates.

(v)   The focus is on a freely supported plate – the methodology can be readily applied to plates with other boundary conditions noting that the optimum shapes may be different.

3. Ls-Dyna Modeling Considerations

Initially, a uniformly thick (i.e. flat) square aluminum plate is considered as a starting shape or baseline design. Initial studies were carried out with the baseline design to better understand the explicit finite element analysis procedure.

Boundary conditions study: Various types of boundary conditions along the plate edges were studied for a freely supported plate, including one or more 'fences' of springs around the edges. While the plate on springs is discussed in Section 7, all these modeling attempts produced unrealistic plastic strain concentrations at the corners. A grip system or assembly that holds the plate was finally adopted owing to best correlation with experimentally observed plate failures (Fig. 2).
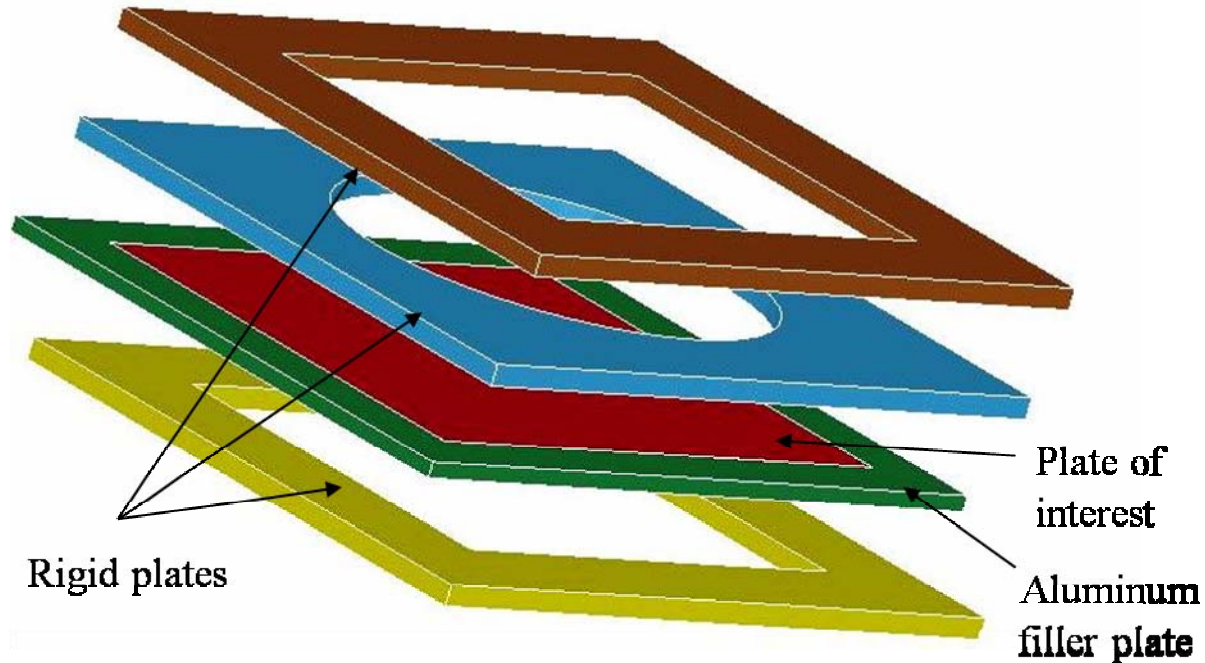
Figure 2. Exploded view of the structure modeled

The whole assembly is free to move during blast. That is, the assembly is unconstrained, to closely simulate blast testing in the field and in pendulum based experiments as noted above. Appropriate boundary conditions using contact surfaces are used to model the assembly. The simulation on the baseline (i.e. flat plate) design produces maximum plastic strain at the center of the plate as also observed in testing. Referring to Fig. 2, components of the grip assembly are:

    i)   the 'plate of interest' (red), made of aluminum.
    ii) a filler plate (blue), also made of aluminum, having same thickness <u>as the edges</u> of the plate of interest, necessary for the assembly.
    iii) three rigid plates, whose material properties are not relevant – steel is assumed for density, and an artificially very high value for Young's modulus is used to ensure rigidity. Importantly, the <u>circular</u> cover plate (blue) above the plate of interest creates peak plastic strain at the center of the flat plate of interest, *as this is the location where a freely supported flat plate is experimentally observed to fail.* That is, without this circular cover plate, as with other modeling attempts mentioned above such as spring supports, unrealistic pseudo concentrations of plastic strains are observed at corners.
    iv) A square portion of the model at the center of plate of interest (red) is taken to be the <u>domain of shape optimization</u>. This square portion lies within the circle of the cover plate (blue). Thus, shape changes (such as bulges) are introduced in this square domain only. The region outside the domain in the plate of interest is flat, whose thickness equals that of the surrounding (blue) filler plate.

It is important to get boundary conditions to model reality as the optimum shape will depend on it. To eliminate the rigid body component, the $w(\mathbf{x})$ in the objective function in Eq. (1) is taken

to be the 'relative' displacement that is obtained by subtracting the nodal displacement at a point in the plate from the displacement of a reference point in the rigid grip.

Elements: All components are modeled using 8-noded hexahedral or brick elements. The 'plate' is thus more a 'solid' since brick elements and not shell elements are used.

Mesh sensitivity study: Further, it is desirable to establish a surrogate model that is computationally efficient and is accurate enough to capture the response trends correctly for iterative optimization. With respect to this problem, the displacement and plastic strain predictions are important. Different mesh densities were chosen in this study. A study was conducted with different mesh densities ranging from 4862 elements to 51902 elements. It was found that peak displacement was not sensitive to mesh refinement, while maximum plastic strain was. The FE analysis time for one complete analysis varied between 90 s for the 4862-element model to 15 min for the 51902-element model when runs were made on a Intel P4-3.6 GHz machine with 3 GB RAM. The simulation time is taken to be the time required for plastic strain to stabilize at a constant value. The coarser FE model was chosen here with appropriately reduced plastic strain limit for constraint evaluation in the optimization problem. Upon solution, a fine mesh of the optimized shape was used to check that plastic strains were less than actual failure limits.

Loading: Blast load exerted is calculated using the ConWep function in Ls-Dyna The inputs for *LOAD_BLAST command are equivalent TNT mass, type of blast (surface or air), load curve, charge location, and surface identification for which pressure is applied. ConWep calculates the appropriate reflected pressure values and then applies these to the appropriate surfaces by taking account the angle of incidence of the blast wave. It should be noted that the loading changes with changes in shape of the plate, although this is automatically calculated during each finite element analysis. Blast parameters are given in Table 1.

Table 1. Blast Load Input Data

Property	Value
Equivalent mass of TNT	1 kg
Blast Location	(0.0,0.0,-0.4064) m
Type of Burst	Air Blast (Spherical Charge)

Material model: The to-be-designed plate and the surrounding filler plate are made of Aluminum 5083 with the bilinear elastic-plastic material model. Material properties are listed in the Table 2. The *MAT_PLASTIC_KINEMATIC input card is used.

Table 2. Aluminum 5083 Material Properties

Property	Value
Mass Density	2700 kg/m^3
Young's Modulus	68.9 GPa
Poisson's Ratio	0.33
Yield Stress	225 GPa
Tangent Modulus	633 GPa
Hardening Parameter	1.0
Failure Strain	0.39

4. Shape Optimization Methodology

Prior to using formal optimization, ad-hoc studies were carried out to generate improved shapes. The following designs were studied:

a) a singly corrugated plate, and

b) a dimpled (indented) plate, with dimples facing towards and away from the charge, respectively.

These ad-hoc attempts, however, did not produce any reduction in maximum deflection and, moreover, lead to rupture levels of plastic strains. Hence, it was decided to use formal optimization methodology.

A square portion of the model at the center of plate is taken to be the domain of shape optimization. That is, shapes changes only occur in this region. This ensures that changes in plate shape do not result in changes in the grip system (see the circular blue cover plate in Fig. 2). However, a thickness change in the design plate has to be matched by an equal thickness change in the filler plate for the assembly to function.

The key equation to implement shape optimization is [11, 12]

$$\mathbf{G}(\mathbf{x}) = \mathbf{G}_{original} + \sum_{i=1}^{N_{dv}} x_i \ \mathbf{q}^i \tag{2}$$

where $\mathbf{G}$ is a grid point coordinates vector, representing x-, y-, z- coordinates of all nodes in the model. Each x_k represents the amplitude of a 'permissible shape change vector' or what is commonly called a 'velocity field' vector $\mathbf{q^k}$. Velocity fields have nothing to do with actual velocities of the model under loading. Vectors $\{\mathbf{q}^k\}$ are generated outside the iterative optimization loop. $\mathbf{G}_{original}$ is the current (flat) shape. Visualization of a $\{\mathbf{q}^i\}$ is identical to visualization of a displacement field in finite elements: $\{\mathbf{q}^k\}$ is multiplied by a magnification scalar and added to the current grid to obtain a displaced grid, except that here the displaced grid represents a new shape and is called a *basis shape*.

The role of the optimizer is to choose $\mathbf{x}^*$ so that the corresponding shape $\mathbf{G}(\mathbf{x}^*)$ is optimum. As $\mathbf{x}$ is iteratively changed by the optimizer, the grid point coordinates $\mathbf{G}$ are updated, a FE input file is then written and an analysis is carried out to evaluate the various functions in the optimization problem. This flow of information may be shown as follows.

Optimizer calls with a $\mathbf{x}^k$ at the kth iteration → construct shape $\mathbf{G}$ from Eq. (2) → Ls-Dyna analysis → evaluate objective and constraint functions → return to optimizer

Chosen Basis Shapes (or Velocity Fields)
Sinusoidal velocity fields for the top and bottom surfaces, independently, are chosen based on the following equation:

$$f(m,n) = C \sin \frac{m \pi x}{L} \sin \frac{n \pi y}{L} \tag{3}$$

where C is a suitable normalization factor and m, n are integers taking on values 1,2,3, etc. In this report, optimization results are presented for two cases – three design variables (denoted 3-DV Case) and nine design variables (denoted 9-DV Case).

3-DV Case: $m = n = 1$. This gives a total of three (3) *symmetric* basis shapes corresponding to
$\quad \mathbf{q}^1 \equiv f(1,1)$ for the top surface,
$\quad \mathbf{q}^2 \equiv f(1,1)$ for the bottom surface,
$\quad \mathbf{q}^3 =$ thickness change
Specifically, $\mathbf{q}^1$ represents a bulge in the shape of the top surface while bottom surface is fixed (other thru-thickness nodes are moved to preserve equal spacing), $\mathbf{q}^2$ represents a bulge on the bottom surface while top surface is fixed, and $\mathbf{q}^3 =$ a thickness change only (that is, middle layer of nodes in the plate are fixed while top and bottom surfaces move in opposite directions). Thus, the design variable vector is $\mathbf{x} = [x_1 , x_2, x_3]^T$, and the optimizer tries to determine an optimum combination of these three basis shapes. Basis shape corresponding to $\mathbf{q}^1$ is illustrated in Fig. 3. Note that the bulge can be positive or negative depending on the sign of x_i
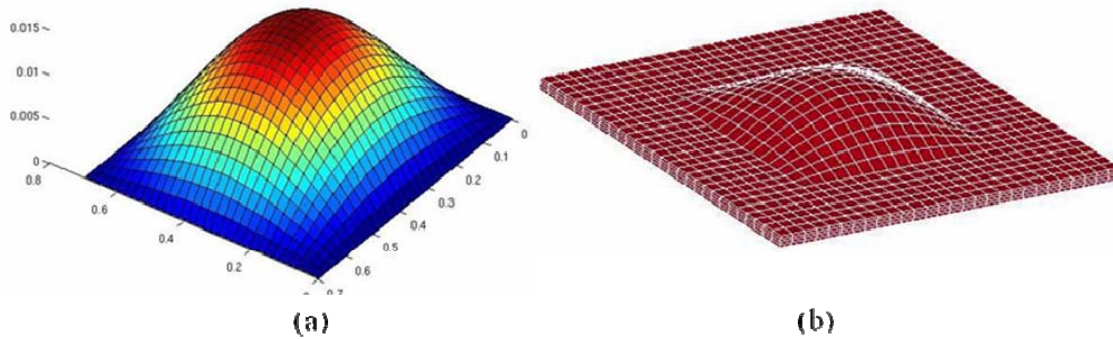

(a)   (b)

Figure 3. (a) Basis shape corresponding to top surface bulge, (b) Basis shape as part of the full plate, showing the domain for shape optimization

2-DV Case: a special case of the 3-DV case where only $\mathbf{q}^1$ and $\mathbf{q}^2$ are used. That is, there is no change in the plate edge-thickness. However, the thickness in the interior of the plate will be non-uniform as these are determined by the relative magnitudes of the bulges created by $\mathbf{q}^1$ and $\mathbf{q}^2$. Note that the plate is modeled using 3-D hexahedral elements and not plate elements.

9-DV Case: $m = n = 2$. This gives a total of nine (9) basis shapes corresponding to

$\mathbf{q}^1 \equiv f(1,1)$, $\mathbf{q}^2 \equiv f(1,2)$, $\mathbf{q}^3 \equiv f(2,1)$, $\mathbf{q}^4 \equiv f(2,2)$ for the top surface,
$\mathbf{q}^5 \equiv f(1,1)$, $\mathbf{q}^6 \equiv f(1,2)$, $\mathbf{q}^7 \equiv f(2,1)$, $\mathbf{q}^8 \equiv f(2,2)$ for the bottom surface,
$\mathbf{q}^9$ = thickness change

Thus, **x** is a (9x1) vector. It should be notes that unlike the 3-DV Case above, presence of unsymmetric basis shapes may lead to an unsymmetric final optimum shape.

5. Optimizers

During computational experiments, it was observed when using a gradient-based optimizer, downhill or descent search directions did not always lead to a reduction in the objective function even for small steps. The problem was seen to be clearly due to non-differentiable functions, attributable to the dynamic nature of the response. Hence the use of gradient based optimizers is not appropriate. The Differential Evolution (DE) technique has proven to be successful [13]. DE is similar to genetic algorithms in some respects such as involving a *population* of designs and having *generations of designs*. DE requires fewer control variables, is robust and is very well designed for parallel computation implementation. Decision parameters of the algorithm are mutation scaling factor and cross over factor for the generation of a population during a new generation. Here, random scaling factor is used for the linear crossover combination of best member and older population, for better diversity. Penalty approach is used to satisfy the constraints. Quadratic penalty is used for plastic strain, geometric and mass constraints, while violation of Jacobian constraint is handled by returning a very high function value since finite element analysis cannot be carried out with a distorted mesh. The total number of finite element analysis is the product of population size and the number of generations. Since DE is stochastic in nature, different seeds have been tried and the best answer based on the minimum objective function value is chosen.

Other optimizers such as a genetic algorithm have also been used. But the DE code performed better for this particular problem. The use of design of experiments (DOE) combined with response surface optimization may be another route to take, however, the nonlinearity of the problem will entail several repeated best-fit surfaces followed by optimization within some iterative scheme. In any vase, parallelization of the DE optimizer makes it viable to directly optimize with accurate Ls-Dyna FE model response.

Parallel Computations

We set the population size equal to ten times the number of design variables. Thus, in the 9-DV case, population size is 90. With the number of generations set as 40, we have a total of 3600 finite element analyses or Ls-Dyna runs. To reduce the total execution time, a simple parallelization of the code using MPI calls has been implemented [14]. We used the LION-XC cluster at Penn State University. Reduction in the total time compared to execution on a single processor workstation makes this optimization approach feasible in the 9-DV case. LION-XC is a cluster with each compute node being a dual 3.0-GHz Intel Xeon 3160 (Woodcrest) Dual-Core Processors

6. Computer Code Development

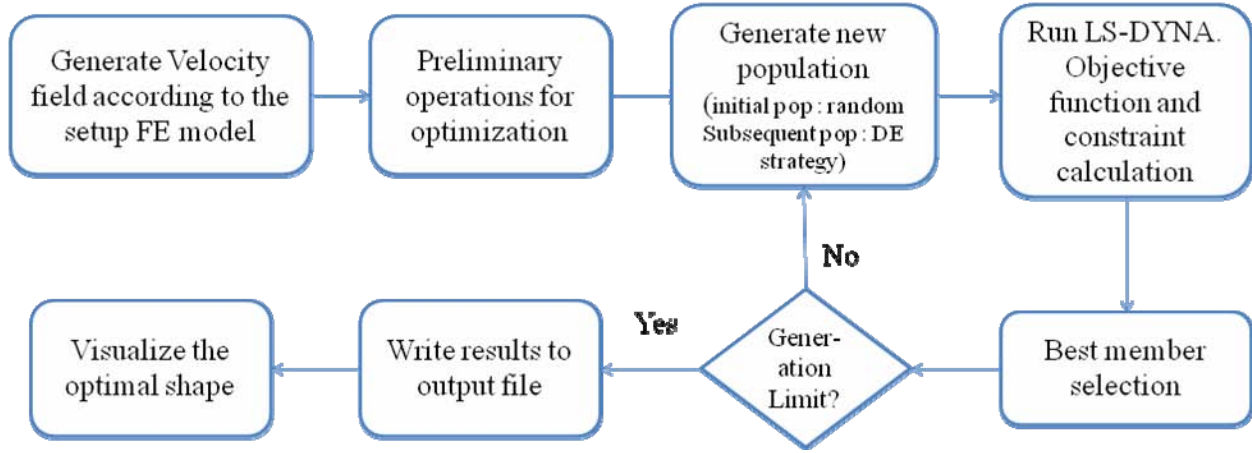A Fortran computer program has been developed to implement the above procedures. The main blocks are shown in Fig. 4.

Figure 4. Flow Diagram of the computer code for shape optimization using Ls-Dyna

A key element of the implementation lies in the creation of two types of input files, as discussed below.

(A) Input File for Design Optimization contains:
- (i) seed used for DE,
- (ii) generation limit,
- (iii) population size,
- (iv) geometric envelope limits (limits for the z-coordinate of the nodes),
- (v) maximum mass limit,
- (vi) plastic strain limit,
- (vii) upper and lower limit of design variable,
- (viii) velocity fields, and
- (ix) model related inputs.

(B) Input File for FE Analysis (Ls-Dyna) contains:
- (i) charge data,
- (ii) material properties, and
- (iii) nodal coordinates and element connectivity.

Typical values used are given in the Table 3. Note that plastic strain limit is less than the material property, to account for the fact that a coarser mesh is being used for optimization (based on the discussion in Section 3). Coordinate files are written for every population generated and checked for distortion of the mesh. High function value is returned for a distorted mesh, otherwise the Ls-Dyna solver is invoked. Ls-Dyna writes nodal and element related time history outputs to ASCII files called 'nodout' and 'elout' respectively. Fortran routines are written to open these files and

calculate relative displacement values and constraint values which are added to objective function as quadratic penalties. Based on the objective function values of all the population members and previous generations, best member is selected and stored. After the last generation, best member is written to the output file along with max displacement value and values of plastic strain. The visualization of the results is through LS-Prepost.

Table 3. Typical values of input parameters used in the input file

Parameter	Value
Generation limit	20 to 45
Population size	30 to 200
Envelope limits (*m*)	-0.3 to 1.0 (large)
	-0.1 to 0.14 (small)
Max mass of assembly (*kg*)	1890.0
Plastic strain limit	0.15
Scaling factor, *C* in Eq. (2)	0.02
Seed	1170, 2349

7. Results - Optimized Panel Shapes

Results using 2-DV, 3-DV and 9-DV (described in Section 4) are presented below followed by physical interpretations and some sensitivity studies. Small variations in the optimized mass from the limiting value is owing to use of exterior penalty functions in the stochastic optimizer.
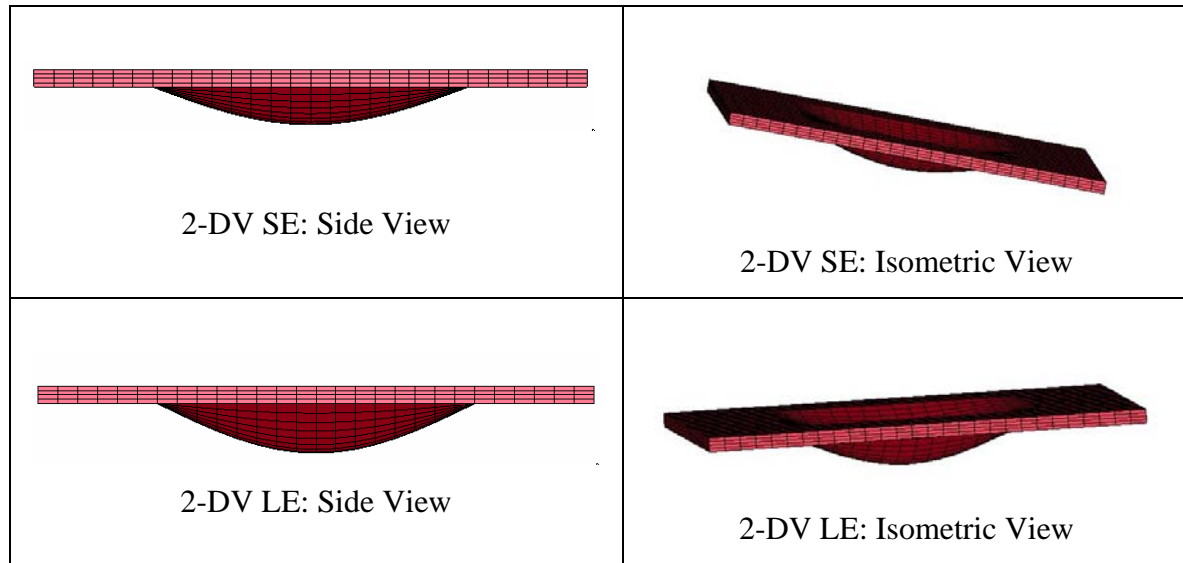
2-DV Case: Results are presented in Table 4, where the edge-thickness of the plate is held constant, using only two velocity fields $\mathbf{q}^1$, $\mathbf{q}^2$. Since edge-thickness is constant, the surrounding filler plate thickness is also unchanged and does not enter into the problem during the iterative optimization process. A single-bulge towards the charge is obtained as optimum (Fig. 5).

Comparing initial and optimized designs, RMS displacement is reduced from 20.51 mm to 5.84 mm, corresponding to a 72% improvement. It may be argued that this comparison is not accurate as there is a difference due to use of penalty functions in the optimizer initial (baseline) mass and optimized mass, viz. between 1872.2 kg and 1899.6 kg (a 1.5% difference). Thus, for a more accurate comparison, the optimized plate is also compared to a flat plate of equal mass. This has been done by adjusting the plate thickness. The total mass of the structure, is maintained at 1899.5 kg, to avoid changes to total baseline impulse, by adjustment of the density of the rigid components whose properties are not relevant except with regard to providing a rigid grip to the

12

plate. It is found that RMS displacement is reduced by 67% (compared to 72% quoted for baseline), plastic strain is reduced by 80% (instead of 84%) and impulse is reduced by 13.3% (compared to 13.7%). Results for both a large envelope (LE) and a small envelope (SE) are presented. The 'large envelope' case is slightly better compared to 'small envelope' case, as is to be expected. Note that the envelope is a user-defined constraint.

Table 4. Optimum solution for 2-DV with Small and Large Envelope

Property	Initial Flat (Baseline) Plate	Optimized 2-DV LE	Optimized 2-DV SE
Population Size in DE optimizer		30	30
Number of Generations in DE		45	45
Max. relative displacement (mm) occurs at 1st peak	58.43	10.5	14.28
Objective = RMS displacement, mm	20.51	5.84	7.34
Max. plastic strain	0.1277	0.021	0.021
Total mass of structure (kg)	1872.2	1899.6	1903.81
Total Z-momentum (kN-sec) (i.e. saturated impulse)	6.254	5.40	5.41

2-DV SE: Side View

2-DV SE: Isometric View

2-DV LE: Side View

2-DV LE: Isometric View

Figure 5. Final optimum shapes with 2-DV where plate edge thickness unchanged

(a single bulge towards the charge)

3-DV Case: Three basis shapes are used here. Initial baseline (flat plate) model and the resulting optimum shape of the panel are shown in Figs. 6a and 6b. The optimized shape turns out to be a double bulge (Figs. 6b, 7) rather than the single bulge in the 2-DV case.
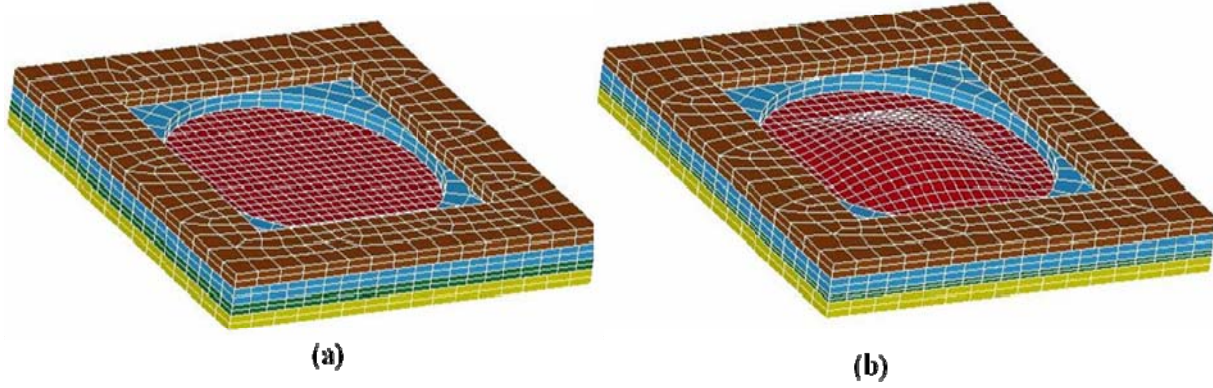

(a)   (b)

Figure 6. (a) Baseline design(uniform thickness) , (b) Optimized plate for large envelope case: double bulge
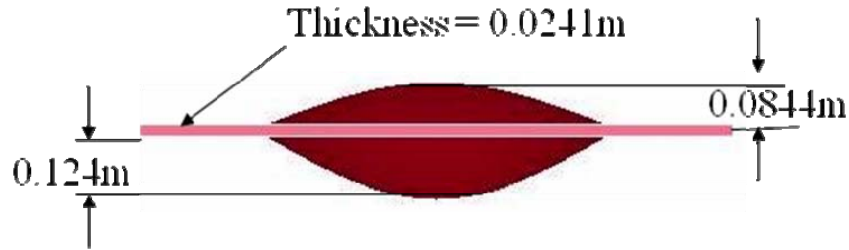

Figure 7. Dimension of the optimal design panel (3-DV large envelope case)

Thickness of the plate of interest outside the shape domain region, which is also the thickness of the filler plate, is reduced from 0.0381 m to 0.0241 m with the introduction of bulges on both sides to keep mass within limits. The result shown in the figures is for the case 'large envelope' where geometric envelope limits are fairly large (relaxed) on both sides. Lower envelope limit cannot be larger than 0.3m due to presence of the charge. With a reduced envelope limit of (-0.1, 0.14) m an optimum double bulge is again seen but lies within the envelope. Table 5 summarizes the results. The 'large envelope' case is slightly better compared to 'small envelope' case, as is to be expected. In Table 5, both RMS displacement, which is the objective function to be minimized, as well as the maximum displacement are quoted. As was done with the 2-DV case, the optimized 3-DV plate is also compared to a flat plate of equal mass. Essentially similar reductions are again observed in RMS deflection, plastic strain and impulse and are omitted for brevity. Displacement reaches its peak at $t = 1.1$ ms.

Plastic strain plots for baseline design and optimized design is given in Figs. 8a, 8b. Plastic strain is maximum at center for the baseline design, as also observed experimentally, while it is around the borders of the domain for the optimized panel (i.e. it is smeared). This demonstrates better utilization of material. Maximum relative displacement of optimized designs versus baseline design is shown in Fig. 9a. The total impulse responses of optimized designs are compared to those of baseline design in Fig 9b. The saturated impulse value of 'large envelope' and 'small envelope' optimized panel designs are 15.6% and 13.6% smaller compared to baseline design, respectively.

Table 5. Results for baseline design and optimized designs for 3-DV case

Property	Baseline Design	Large Envelope (-0.3,1.0)m		Small Envelope (-0.1,0.14)m	
		Optimized Design	*Change*	*Optimized Design*	*Change*
Objective Function (*m*)	20.51E-03	4.34E-03	78.9%	4.49E-03	78.1%
Max Relative Displacement (*m*)	58.43E-03	7.32E-03	87.5%	7.68E-03	86.9%
Max plastic strain	0.1277	0.01932	84.9%	0.02028	84.1%
Total Mass (*kg*)	1872.2	1894.57	(1.2%)	1894.54	(1.2%)
Saturated impulse, (*kg-m/s*)	6254.3	5298.62	15.6%	5425.82	13.6%

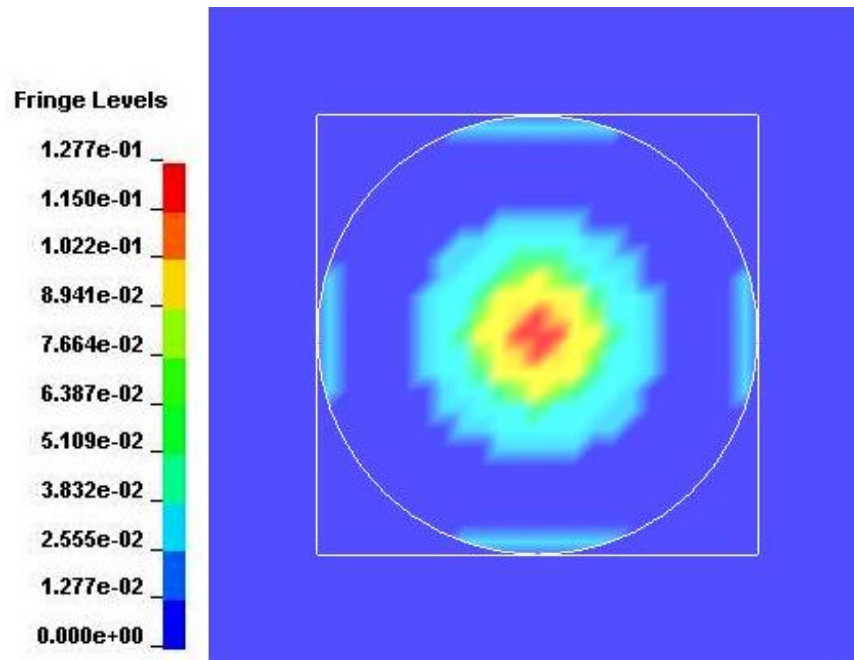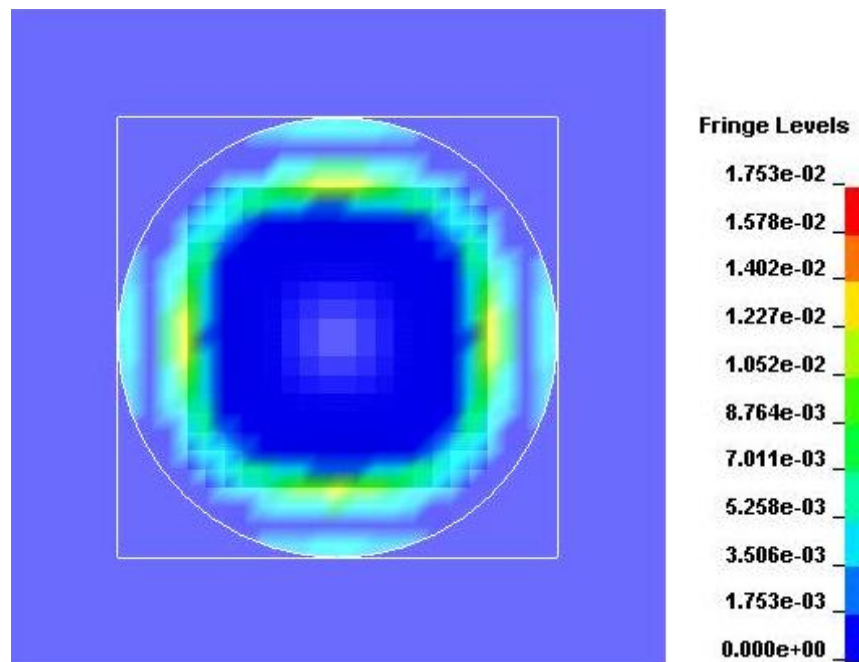**Figure 8a. Plastic strain plot for initial baseline (flat plate) design**

Figure 8b. Plastic strain plot for 3-DV large envelope optimized design
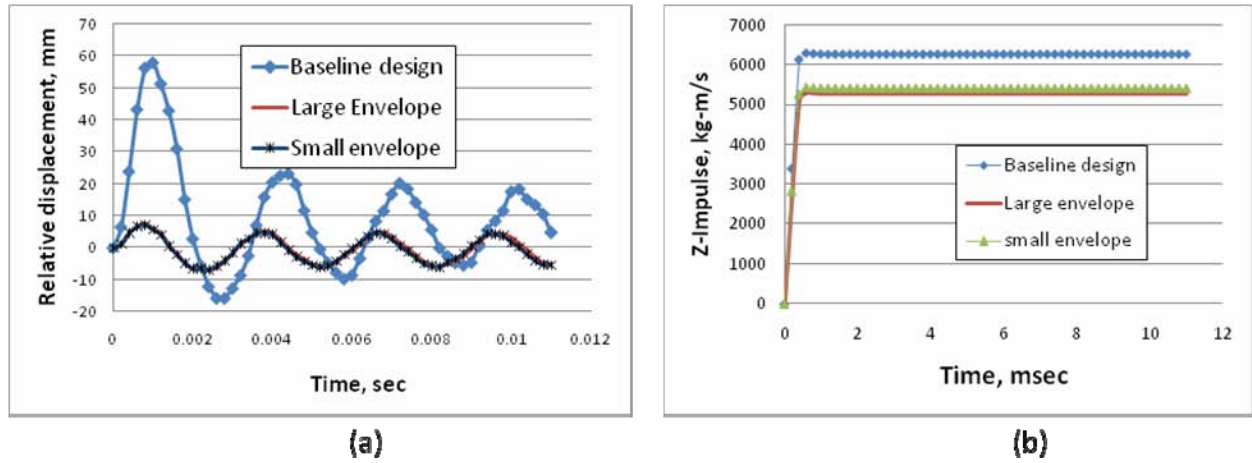
Figure 9. (a) Comparison of relative displacement, (b) Comparison of impulse response

Table 6 compares the 3-DV large envelope case to the 2-DV large envelope case. While the final masses are a little different, the 3-DV case is better than the 2-DV case even with lesser structural mass.

Table 6. Comparison of Optimized Plate and Flat Plate of Equal Mass

Property	Flat plate of equal mass	Large Envelope (-0.3,1.0)m		Small Envelope (-0.1,0.14)m	
		Optimized Design	*Change*	*Optimized Design*	*Change*
Objective Function (*m*)	1.32E-02	4.34E-03	67.12%	4.49E-03	65.98%
Max Relative Displacement (*m*)	3.88E-02	7.32E-03	81.15%	7.68E-03	80.23%
Max plastic strain	0.08739	0.01932	77.89%	0.02028	76.79%
Total Mass (*kg*)	1894.5	1894.57	0.00%	1894.54	0.00%
Saturated impulse, (*kg-m/s*)	6229.3	5298.62	14.94%	5425.82	12.90%

Physical Interpretation of Results of 3-DV case: The bottom bulge towards the charge, observed in both 2-DV and 3-DV optimized shapes, is likely playing an important role in deflecting blast waves away from the panel. The 3-DV result achieves greater reduction compared to the 2-DV result by adding material to the center while simultaneously thinning the plate to keep mass constant, what may be termed a 'mass effect'. The amount of material added can be controlled by the designer by suitably defining the envelope limits.

3-DV Optimization of a plate supported on the four edges on springs

       Results for a plate <u>without the grip assembly</u> and supported on edge springs (mimicking a freely supported / lightly clamped conditions) are presented in Table 7. We observe, again, the double bulge shape (Fig. 10) and large improvements over the baseline design. However, as noted in Section 3, this plate support system was discarded in favor of the grip system presented earlier owing to plastic strain concentrations near the corners, inconsistent with experimental observations. The purpose of presenting this result is to lend further credibility to the optimized shaped obtained above.

Table 7. Optimum solution of plate with springs with 3-DV

Property	Baseline (Flat)	3DV SE	3DV LE
Population Size		30	30
Number of Generations		20	20
Max. relative displacement (mm) occurs at 1st peak	86.2	31.3	28.2
Objective = RMS displacement, mm	46.8	23.1	21.8
Max. plastic strain	0.055	0.126	0.149
Total mass of structure (kg)	152.9	147.01	149.87
Total Z-momentum (kN-sec)	4.93	3.7	3.6

3DV SE

3DV LE

Figure 10. Final optimal shape for plate with spring supports with 3-DV

9-DV Case: We now present optimization results with 9 basis shapes. The best shape obtained by the optimizer (repeated trials were needed) is shown in Fig. 11, which is again seen to be a double bulge, albeit slightly non-symmetric in the 9-DV case owing to the optimizer. Comparison with 3-DV Case is given in Table 8 for the small envelope case. Results obtained show only marginal improvement over 3-DV Case. The 9-DV Case is a very challenging task for any optimizer. It may still be that a hitherto undetermined unsymmetric sinusoidal shape lies within the design space that has a lower objective. However, we have a fair amount of confidence in the result obtained below owing to the use of various starting random number seeds. Further, optimal shapes that are 'wavy', even if discovered in the future, are hard to manufacture and may be very sensitive to charge location.

Table 8. Comparison of 3DV and 9DV Cases

Property	3 dv	9 dv
Objective function value (m)	4.49E-03	4.28E-03
Max relative displacement (m)	7.68E-03	7.79E-03
Max plastic strain	0.020282	0.02233
Total mass of the structure (kg)	1894.54	1895.3
Impulse (Ns)	5401.41	5313.58

Figure 11. Optimum shape corresponding to 9DV Case

Sensitivity to charge, standoff distance: Limited sensitivity studies were conducted to ensure that the optimum shapes did not change with ±5 % and ±10 % changes in standoff distance (z-distance of charge from plate) and also of charge amount (i.e. kg of TNT). For brevity, details are not given here, since the optimized shapes and results are similar except for small perturbations in values. As the standoff distance decreases, bulge towards the charge was larger compared to the amount of bulge on the top face of the panel. With the increases in standoff distance, the optimum shape remained same.

8. Off-Center Charge Locations

The optimization is carried out in four 'steps', each successively offsetting the charge by a distance of $L/24$ (L being the length of the plate of interest) along the x-axis from the initial center position. The y, z co-ordinates remain the same at 0, -0.4064 m respectively. In each subsequent step the previous step's optimized shape was used as the initial shape. 11 and 7 basis shapes are used, respectively, for unsymmetric and symmetric shape variations. Shape morphosis as a result of charge off-set is shown in Fig. 12. Step 3 onwards a cavity appears on the bottom surface of the plate over the $-x$-axis. The thickness (bulge) of the plate increases until the mass limit is reached. Thereafter a cavity is formed to get more mass above the charge location. The C.G. of the plate shifts in the direction of the off-center charge. Figure 13 shows this cavity in detail. Table 9 contains the response values.

Center Charge   *Step 1*   *Step 2*

Step 3   *Step 4*

Figure 12. Right Profile View of the Optimized Plates with increasing charge offset (towards the left, in steps of $L/24$ from center, L = length of 'plate of interest')

Figure 13. Cavity appearance in Step 4, at bottom of plate
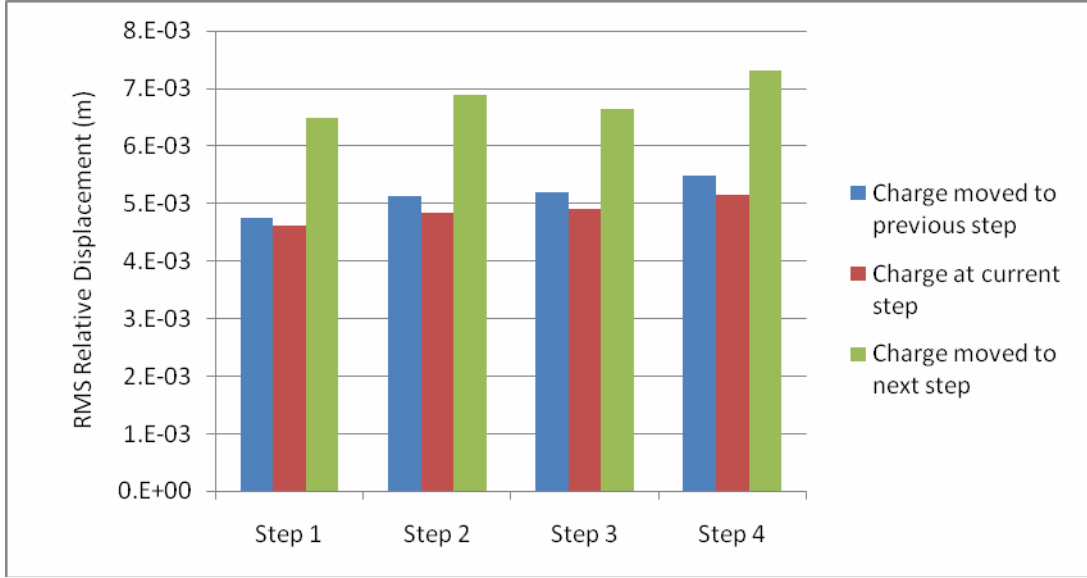
Table 9. Results with offset charge

Charge Location	Objective = RMS Relative[1] Displacement (mm)	Max Plastic Strain[2]	Total Mass of the assembly (kg)
Center	4.48	0.0231	1894.54
Step 1 (L/24)	4.62	0.0367	1895.52
Step 2 (L/12)	4.83	0.0361	1891.77
Step 3 (L/8)	4.91	0.0293	1894.25
Step 4 (L/6)	5.15	0.0440	1893.00

[1]Relative Displacement = δ - $\delta_{fixture}$ at 1st peak
[2] Limit value used is 0.15

A verification study of optimality for offset charges: Owing to the difficulty in using the stochastic optimizer on this problem, a coarse verification on optimality is carried out by shifting the charge a step backward (along *x*-axis) and a step forward for each step. It is verified that the shape obtained for each step is best for the charge location for which it was optimized. Another way of interpreting the results is that for a given charge position the shape optimized for it is better than either of the adjacent step shapes. A chart of the verification results is provided below in Table 10.

Table 10. Verification study of optimality for offset charges

9. Methodology development for optimization of honeycomb sandwich structure

Lightweight, high strength and high energy absorbing materials are most suitable for protective structures against blast loading. It is well known that metal sandwich plates have proved to serve this purpose and honeycomb sandwich material is a suitable option. For maximum benefit, different parameters of honeycomb core sandwich metal plate need to be optimized. However, modeling the each cell in the honeycomb core in detail with iterative optimization techniques is computationally infeasible. Instead, the viable approach adopted here is to replace the honeycomb core with a solid plate with *equivalent* mechanical properties. A novel strategy is developed here to optimize the honeycomb sandwich structure based on two concepts: (1) Parameterization of the unit cell in terms of a finite number of design parameters, a subset of which are selected as design variables for optimization after carrying out a numerical study, and (2) V*irtual testing*, a novel technique developed here, to link or characterize the stress-strain curve as a function of the design variables, paving the way for subsequent optimization.   These two concepts are detailed below in the context of air blast mitigation.

Honeycomb core unit cell geometry: The honeycomb core sandwich structure considered here consists of three layers: top metal face plate, honeycomb core (Fig. 14), and bottom metal face plate. Honeycomb core is characterized by its cell size D, foil thickness t, branch angel α, and core thickness h. All these parameters decide its crush strength, which is the key property for offering protection against the blast load. In this study we consider the regular hexagon cell core, $\alpha = 120^0$, as it gives maximum crush strength [15]. The face plates are characterized by their thicknesses, but these enter only at the final stage during optimization of entire structure and are not relevant to parametrization of the core. Figure 15 shows the triangular unit cell that has been used in this study. Figures 15(b) and 15(c) show the full model and cross section of the model, respectively.
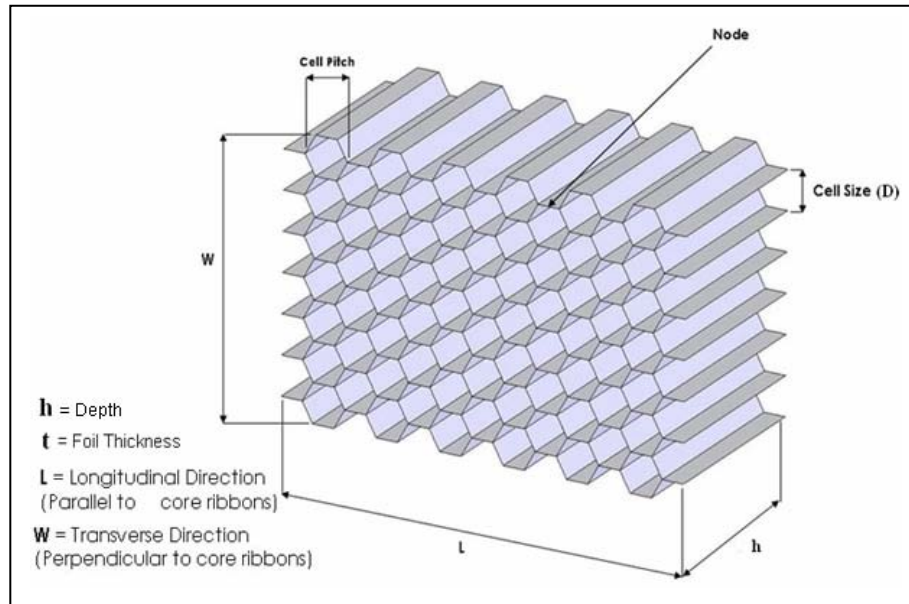
22

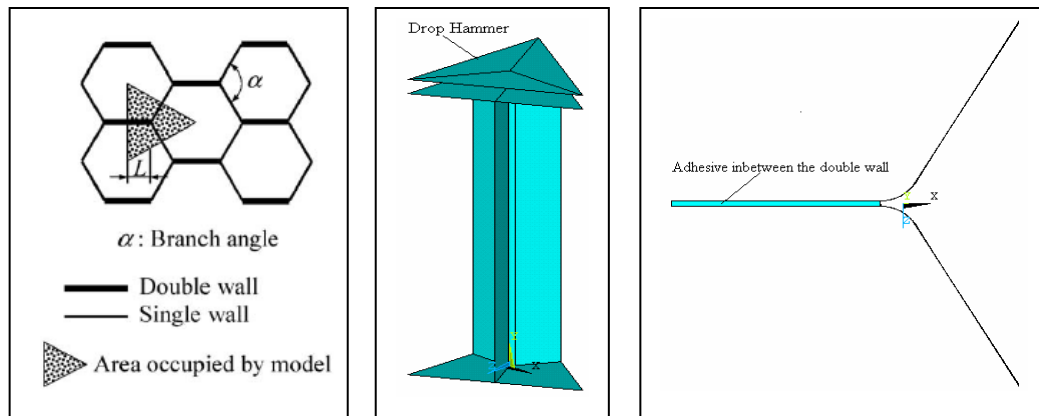**Figure14. Schematic view of honeycomb core geometry**

Figure 15 *a - c*. Unit cell model of honeycomb core

Virtual testing of Unit Cell

      A novel strategy, V*irtual Testing*, is used to characterize the stress-strain curve as a function of the design variables, paving the way for a subsequent optimization study The crush test is carried out using LS-Dyna. The foil is modeled by quadrilateral Belytschko-Tsay shell elements and the adhesive layer of 0.01mm thick at the double wall is modeled using solid brick elements. A5052 aluminum alloy is used for the foil in the study. Bilinear isotropic material model (Table 11) is used for the foil and the adhesive. Automatic single surface contact is applied to the model with sliding and sticking frictional coefficients as 0.2 and 0.3 respectively [15]. Figure 16 shows four different stages of crushing of honeycomb core. Buckling of the foil

23

(cyclic folding) starts from near the impact edge and propagates downward as the hammer travels. Figure 17 shows the variation of nominal compressive stress with the volumetric strain (hammer travel). Compressive stress is defined as the reaction force experienced by the hammer divided by the whole cross sectional area and the volumetric strain is calculated by the change in core depth divided by its original value. The core resists to buckling until the peak stress point and then undergoes cyclic collapse of the foil as the hammer travels. The crush stress is the average of the oscillatory stress during the cyclic collapse of the foil. Once the entire core is folded, then densification starts resulting in very high compressive stress. The crush stress is a vital property which reduces the blast shock transmission by absorbing the energy and hence minimizes the damage to life. Although sufficient care is taken while approximating the load curve, it is not possible to define the crush start and end strain with great accurately.

Table 11. Mechanical properties of materials used in the modeling of the unit cell

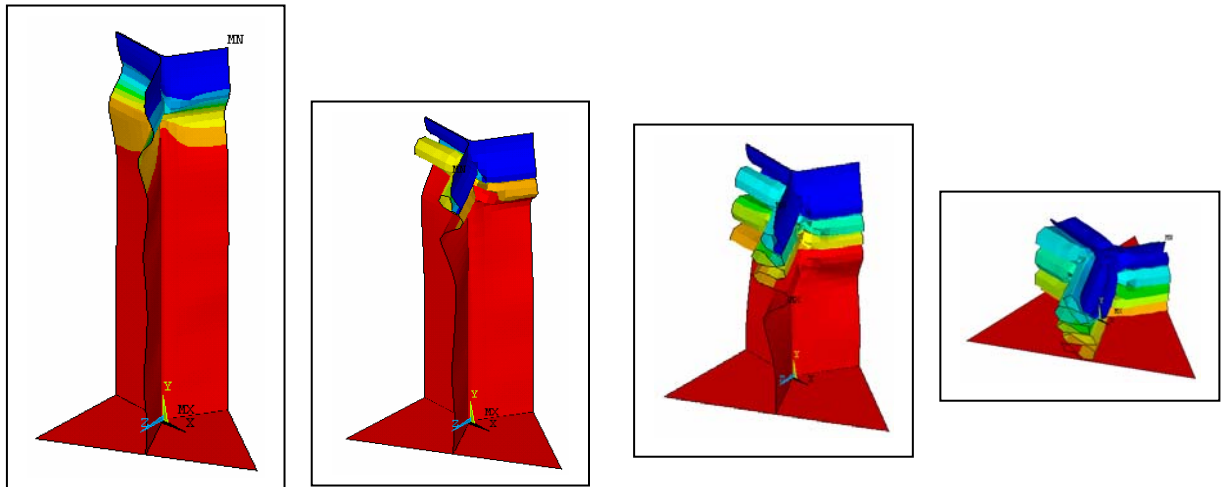| Material	Density (Kg/ m^3)	Young's Modulus (GPa)	Yield Stress (MPa)	Tangent Modulus (GPa)	Poison's Ratio
A5052	2680	72	300	50	0.34
Adhesive	2000	5	30	0	0.3
Rigid metal	288E5	200	-	-	0.24

Figure 16. Virtual Testing simulation of gradual crushing of the honeycomb core
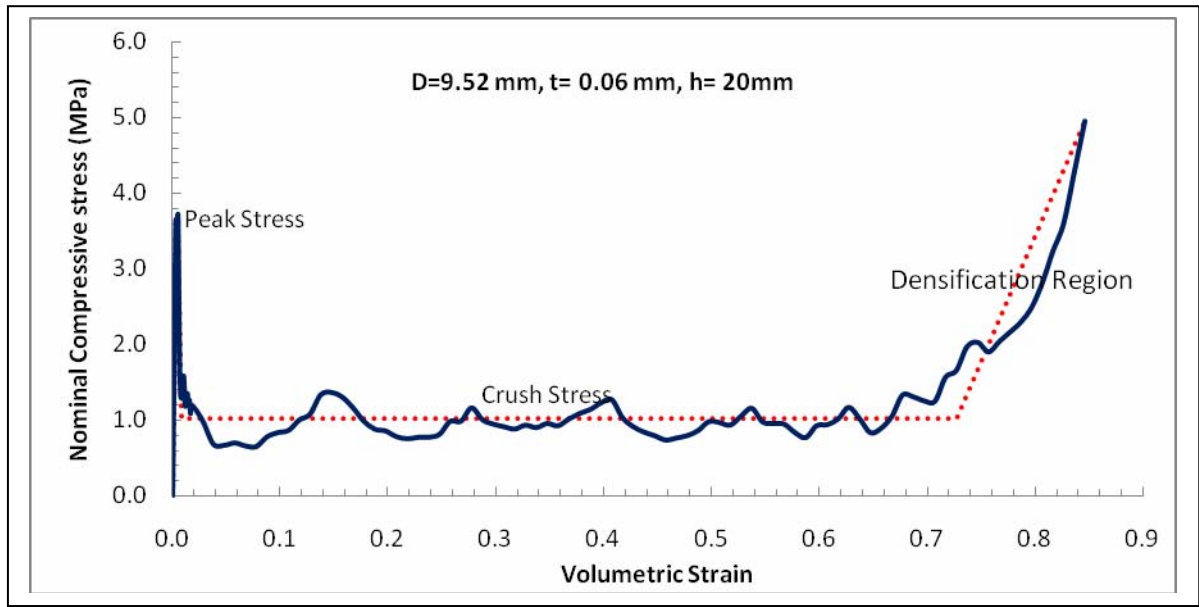
Figure 17.   Load curve and its different parameters of honeycomb core

Effect of different test parameters on load curve: Three different element sizes (Fig. 18) are used to study their effect on the load curve. No noticeable change is observed when element size is increased from 0.25mm to 0.5mm. Load curve doesn't shows any visible change (Fig. 19) with the change of core depth from 20mm to 50mm. However, at a lower core depth such as 5mm, densification starts early. But the crush stress is not affected by the variation of core depth. For better design, the core depth should be sufficient enough to allow few cyclic folding of the foil during crushing. Figures 20 and 21 shows the effect of the cell size D and foil thickness t on the load curve. Crush stress decreases with cell size and increases with foil thickness. Parametric study is carried out by varying the cell size and the foil thickness, the element size and the core depth are kept constant as 0.4mm and 20mm respectively.

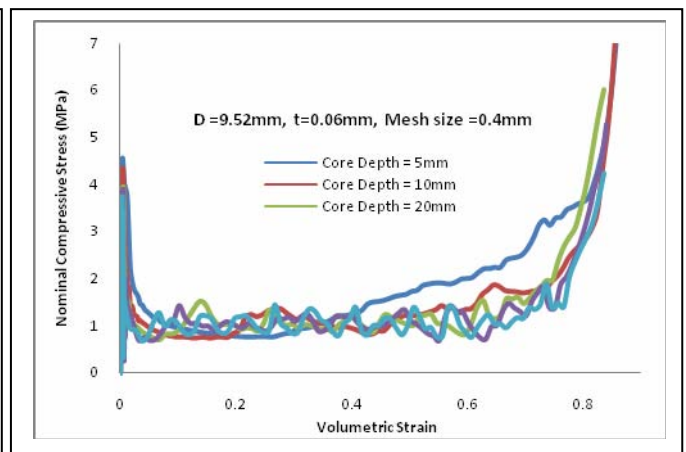
Figure 18: Effect of mesh size on load curve
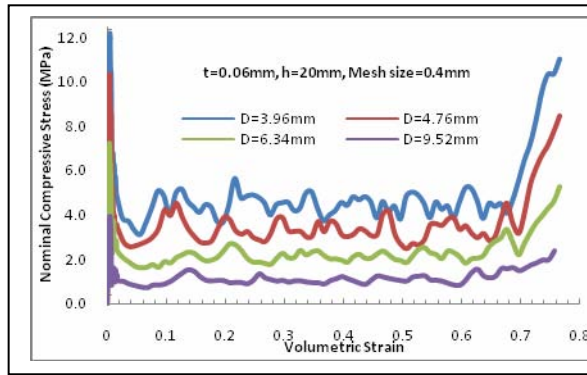

Figure 19. Effect of core depth on load curve

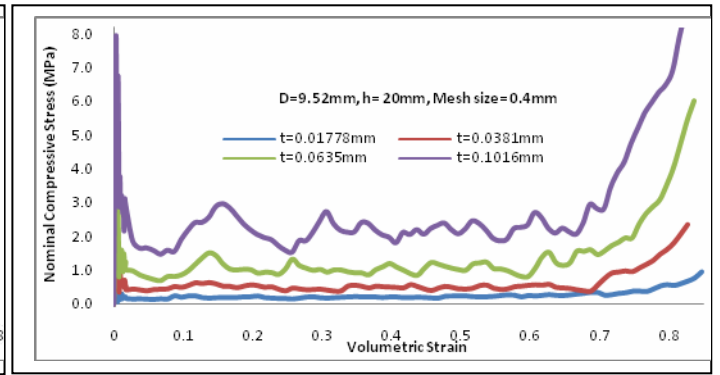**Figure 20. Effect of cell size on load curve**

Figure 21. Effect of foil thickness on load curve

Parameterization the load curve in terms of design variables: Crush start and end strain doesn't show much change with *D* and *t*, hence they can be assumed to be independent. The area under the load curve mostly depends upon the value of crush stress and doesn't change much with a small error in determining peak stress, peak strain, crush start and end strain. Peak stress, crush stress (Fig. 22) and final stress (Fig. 23) are expressed in terms of dimensionless parameter; *t/D* and trend lines are added. All the curves fit well and the relations match well with Ref. [16]. The tensile stress cut off is taken as the average of the final stress and the crush stress. With these relations, a load curve can be expressed for a particular value of *D*, *t*. Above analysis leads to a load curve shown in Fig. 24 expressed in terms of *D*, *t*.
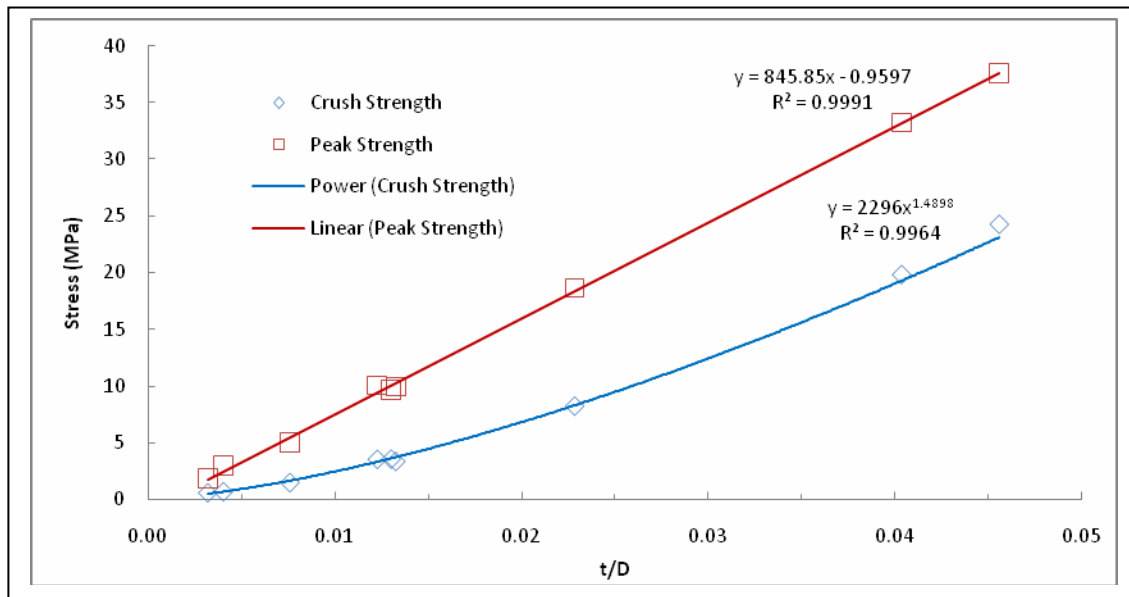

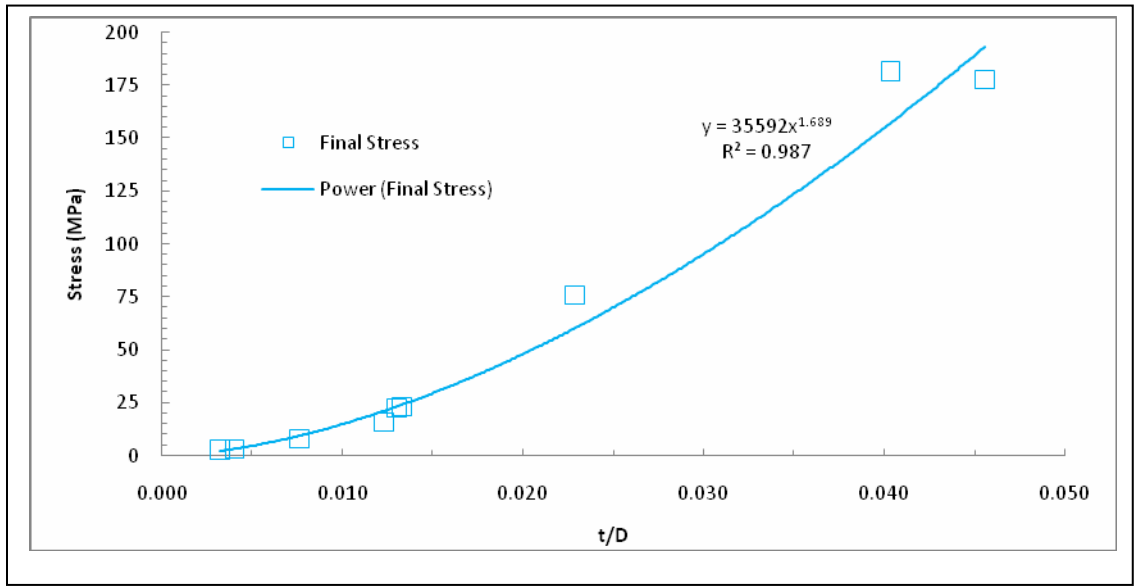**Figure 22. Parametric form of crush stress and peak stress**

26

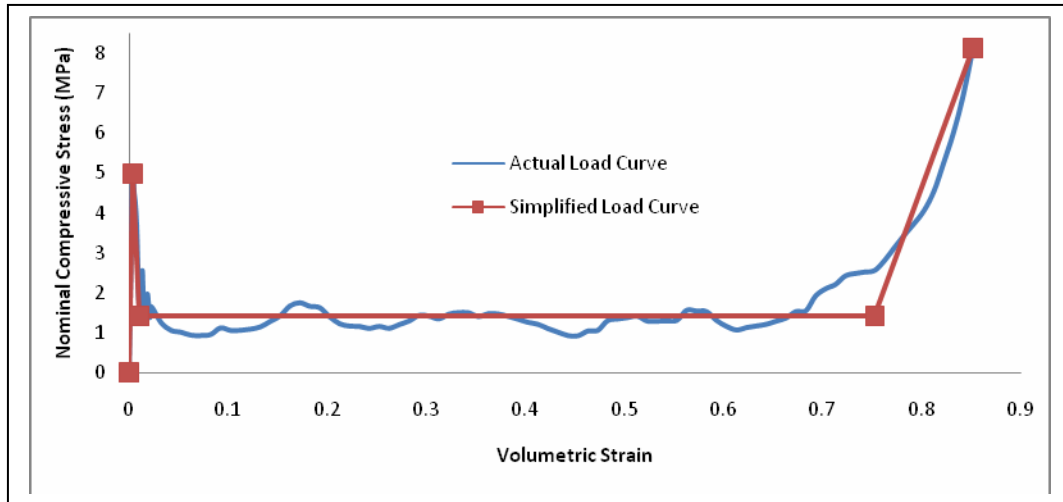**Figure 23. Parametric form of final stress**

Fig-24: Load curve used for the honeycomb core

Analysis of a base line model (without optimization): Figures 25 and 26 shows two types of test models of comparable weight. Figure 25 is the model used earlier in the report, for an all-aluminum structure. No optimization is used here. However, this analysis demonstrates that optimization can have significant benefits. Material properties used in the model are shown in Table 12. Blast load of 8 kg mass of TNT is applied from a 0.4064m distance from the centre of the bottom face of the plate and the results are analyzed.
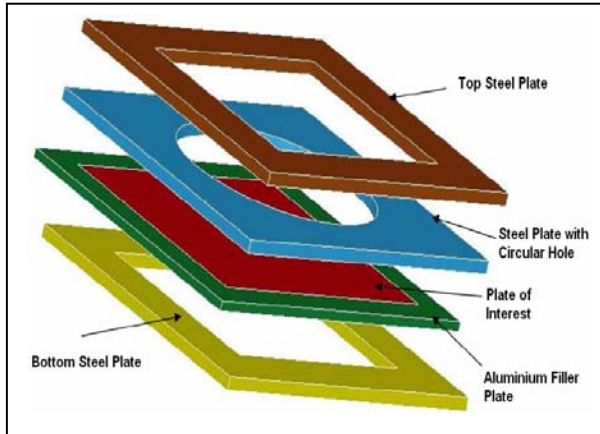
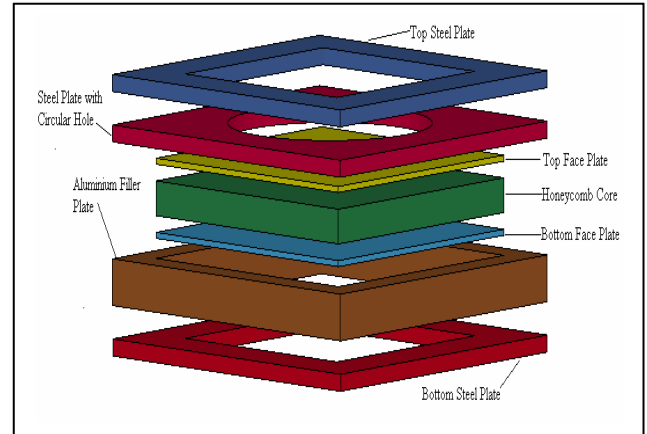**Fig-25: Test model for solid plate sandwich core**

Fig-26: Test model for honeycomb

Table 12. Material properties for the model

Material	Density (Kg/ m^3)	Young's Modulus (GPa)	Yield Stress (MPa)	Tangent Modulus (GPa)	Poison's Ratio	Tensile Stress Cut Off (MPa)
A5083	2700	68.9	225	0.633	0.33	--
Honeycomb Core (A5052)	54.05	1.28	--	--	0	6.05
Steel 4340	8257.85	2080	1010	0.25	0.29	--

Results and discussion of analysis: In the sandwich model, maximum z-displacement and effective plastic strain occurs at the bottom face plate (Figs. 27, 28 and Table 13). The blast shock transmits to the honeycomb core through the bottom face plate and hence bottom face plate undergoes maximum displacement and plastic strain. Most part of the blast shock is absorbed by the honeycomb core, as a result of that top face plate is protected (Fig. 29). The basic idea of honeycomb core plate design is to protect the structure facing towards the human life. The maximum displacement of the top face plate is less than that of plate model by 26%. The displacement of the plate in plate model is more oscillating in nature (Fig. 9) where as it is very smooth (Fig. 27) in the honeycomb core model, which indicates that major part of the shock is absorbed by the honeycomb core. The effective plastic strain of the top and bottom face plate (Table 13) is one order less than that of plate model. This is because of the fact that top and bottom face plates are loosely constraint due to easily deformable nature of the honeycomb core. This low effective plastic strain would give us a larger limit for shape optimization without

violating the plastic strain limit. Scope for size and shape optimization of the honeycomb sandwich structure is given in Section 10 below.
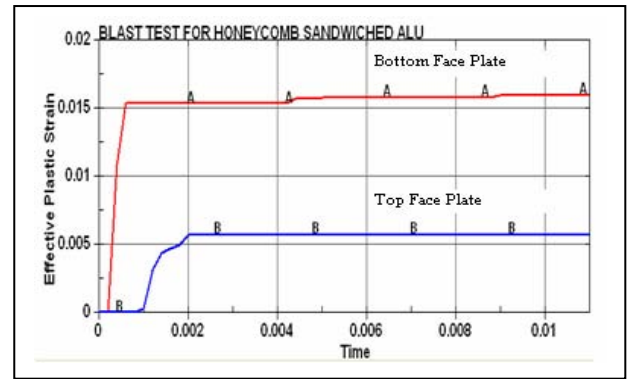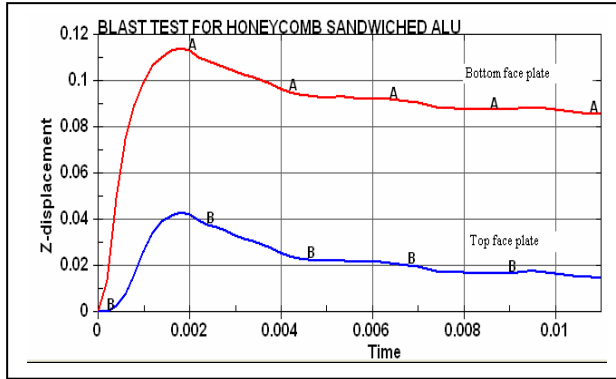

Figure 27. Max displacement of the face plate   Figure 28. Max effective plastic strain of face plate

Table 13. Result summary of both the models

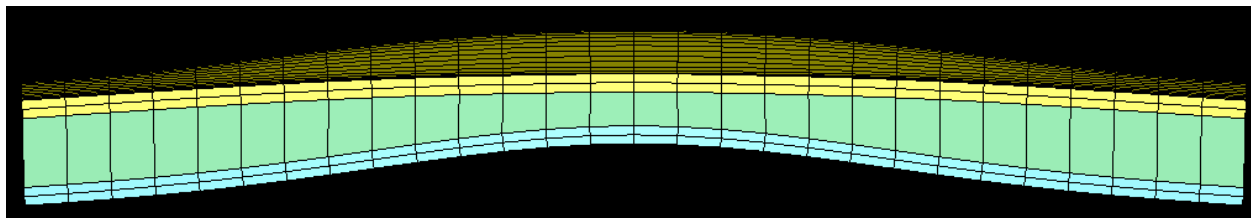| Model type	1st Peak relative Z-displacement (mm)		Maximum effective plastic strain	
Honeycomb model	Bottom face	Top face	Bottom face	Top face
	114	43	0.016	0.0057
Plate model	58		0.124	

Figure 29. Deformation of the honeycomb sandwich at the 1st peak

10. Conclusions and Future Research

Shape optimization of a freely supported solid aluminum panel for air blast load mitigation is carried out. Center and off-center charge locations are considered. This research is timely as very little work has been done in this area. Ls-Dyna is coupled to a stochastic DE optimizer using a modular Fortran code that has been developed. Thus, accurate responses are used at all times during optimization. Parallelization of the DE optimizer makes the optimization approach viable. The finite element model has been developed to reflect experimental test conditions and observed structural response. Two, three, and nine sinusoidal basis shapes are chosen, respectively. The optimum shape, a combination of these basis shapes, turns out to be a single-bulge toward charge in the 2-DV case likely attributable to a deflection of blast waves. In the 3-DV and 9-DV cases, there is a double bulge, where material is added to the center of the plate with simultaneous thinning of the plate. This shape may be explained as a combination of deflecting the wave and a mass effect. The shape and results are robust with respect to small changes in charge density or standoff distance. A plate on springs, with no grip system also results in a double-bulge shape.

Importantly, at optimum, the plastic strain is smeared, indicating better utilization of the material. The panel's RMS displacement which is the objective function, relative to the fixture, is significantly decreased (80% compared to the baseline design, and 67% compared to a flat plate of equal mass). Saturated z-impulse decreased by 14%. Maximum plastic strain decreased significantly as well (and smeared around the edges) and was well within the limit. Results have also been verified using a finer mesh for optimized shapes.

A morphosis of optimized shapes for increasing off-set of charge location show that the characteristic double bulge shape remains with the bottom bulge shifting with the charge. Beyond a certain off-set value, the optimized shape changes in character, where a bottom cavity is formed away from the charge in order to get more mass above the charge location. The C.G. of the plate shifts in the direction of the off-center charge.

Methodology for optimization of honeycomb sandwich structures is developed. Geometry parameters describing honeycomb core geometry are linked with the stress-strain curve and thereby to Ls-Dyna input parameters, using a novel idea based on virtual testing. Here, virtual testing involves crushing a unit cell using Ls-Dyna again. Studies are conducted for varying values of core geometry parameters leading to regression formulas that provide the needed relationships between geometry and analysis inputs.

The task of finding a global optimum in such highly nonlinear, nonconvex and computationally expensive functions is challenging and improved optimizers are needed in future. The honeycomb optimization methodology developed here needs to be coupled to simultaneous size and shape optimization of the composite structure, involving thicknesses of face plates and core depth, core geometry, and shape of outer boundary of face plates. The ability of the honeycomb core to absorb energy reduces plastic strain in the top face plate away from the charge thus leaving significant room for optimization of the sandwich structure.

This work lays down a methodology of structural shape optimization against blast loading.

References
[1] Dharaneepathy. M.V and Sudhesh. K. G "Optimal Stiffening of square plates subjected to air-blast loading", Computers & Structures. Vol 36.No.5, 891-899, 1990.

[2] Hou, Hai-Liang, "Study on failure mode of stiffened plate and optimized design of structure subjected to blast load", Explosion and Shock Waves [in Chinese], Vol. 27, 26-33, 2007.

[3] Xue, Z. and Hutchinson, J.W., " A comparative study of impulse-resistant metal sandwich plates", International Journal of Impact Engineering, 30, 1283–1305, 2004.

[4] Fleck, N.A. and Deshpande, V.S., "The Resistance of Clamped Sandwich Beams to Shock Loading", Vol. 71, J. of Applied Mechanics, Transactions of the ASME,   386-401, May 2004.

[5] Yen. C.F, Skaggs. R, Cheeseman, B.A., "Modeling of shock mitigation sandwich structures for blast protection". The 3rd First International Conference on Structural Stability and Dynamics, Kissimmee, Florida, June 19-22, 2005.

[6] Liang, C.C., Yang, M.F., Wu, P.W., "Optimum design of metallic corrugated core sandwich panels subjected to blast loads", Ocean Engineering, 28, 825–861, 2001.

[7] Main, J.A. and Gazonas, G.A., "Uniaxial crushing of sandwich plates under air blast: Influence of mass distribution", International Journal of Solids and Structures, 45, 2297–2321, 2008.

[8] Icardi, U. and Ferrero, L., "Impact and blast pulse: Improving energy absorption of fibre-reinforced composites through optimized tailoring", Proceedings of ESDA 2006, 8th Biennial ASME conference on Engineering Systems Design and Analysis, Torino, Italy, July 4-7, 2006.

[9] S.C.K. Yuen and G.N. Nurick, "Experimental and Numerical Studies on the Response of Quadrangular Stiffened Plates. Part I: Subjected to Uniform Blast Load", Intl J of Impact Engineering, 31, 55-83, 2005.

[10] G.S. Langdon, S.C.K. Yuen and G.N. Nurick, "Experimental and Numerical Studies on the Response of Quadrangular Stiffened Plates. Part II: Localised Blast Loading", Intl J of Impact Engineering, 31, 85-111, 2005.

[11] Belegundu, A.D, and Chandrupatla, T. R., Optimization Concepts and Applications in Engineering, Prentice-Hall, New Jersey, 1999.

[12] Belegundu, A.D. and S.D. Rajan. "A Shape Optimization Approach Based on Natural Design Variables and Shape Functions", J. Computer Methods in Applied Mechanics and Engineering, 66:87-106, 1998.

[13] Price, K. and Storn, R., "Differential Evolution (DE) for Continuous Function Optimization", http://www.icsi.berkeley.edu/~storn/code.html.

[14] S.D. Rajan and D.T. Nguyen, "Design Optimization of Discrete Structural Systems Using MPI-enabled Genetic Algorithm", Journal of Structural and Multidisciplinary Optimization, 27, 1-9, 2004.

[15] Yamashita M. and Gotoh M. (2004) Impact behavior of honeycomb structures with various cell specification-numerical simulation and experiment. International Journal of Impact Engineering, 32, 618-630.

[16] Wu Enboa and Jiang Wu-Shung (1996) Axial crush of metallic honeycombs. International Journal of Impact Engineering, 19, 439-456.